Predicting vacancy-mediated diffusion of interstitial solutes in α-Fe

Caroline Barouh, Thomas Schuler, Chu-Chun Fu,[*] and Thomas Jourdan

CEA, DEN, Service de Recherches de Métallurgie Physique, F-91191 Gif-sur-Yvette, France

Based on a systematic first-principles study, the lowest-energy migration mechanisms and barriers for small vacancy-solute clusters ($V_n X_m$) are determined in α-Fe for carbon, nitrogen, and oxygen, which are the most frequent interstitial solutes in several transition metals. We show that the dominant clusters present at thermal equilibrium (VX and VX_2) have very reduced mobility compared to isolated solutes, while clusters composed of a solute bound to a small vacancy cluster may be significantly more mobile. In particular, $V_3 X$ is found to be the fastest cluster for all three solutes. This result relies on the large diffusivity of the most compact trivacancy in a bcc lattice. Therefore, it may also be expected for interstitial solutes in other bcc metals. In the case of iron, we find that $V_3 X$ may be as fast as or even more mobile than an interstitial solute. At variance with common assumptions, the trapping of interstitial solutes by vacancies does not necessarily decrease the mobility of the solute. Additionally, cluster dynamics simulations are performed considering a simple iron system with supersaturation of vacancies, in order to investigate the impacts of small mobile vacancy-solute clusters on properties such as the transport of solute and the cluster size distributions.

PACS number(s): 61.72.S−, 66.30.J−, 61.72.jd, 31.15.A−

I. INTRODUCTION

Small interstitial elements are always present in metals. For example, the most frequent interstitial impurities in iron and other transition-metal systems are carbon (C), nitrogen (N), and oxygen (O). Also, C and occasionally N and O are added to iron to make steels. It is now well established that these solutes interact strongly with vacancies (V), the most common structural defect, and tend to form highly stable vacancy-solute clusters ($V_n X_m$) [1–9]. As raised in previous studies, even a very small amount of the interstitial atoms may have significant effects by increasing vacancy concentrations and decreasing their mobility [10–13]. On the other hand, even if interstitial atoms can diffuse throughout the lattice without being assisted by vacancies, unlike substitutional solutes, vacancies may still influence the transport and clustering of the solute elements. For instance, under irradiation, vacancies interfere with the precipitation of carbides [14–17]. However, quantitative information of how their diffusion may be modified by the presence of neighboring vacancies is still lacking.

Clusters made of interstitial solutes and vacancies are generally believed to have reduced mobility with respect to isolated vacancy or solute. Previous computer simulations and interpretation of experiments on kinetic properties of interstitial solutes and defects in metals mostly assumed that $V_n X_m$ clusters are immobile [6,12,13,18,19]. At the atomic scale, the migration energy of the isolated solutes and some relevant solute jump barriers in VX pairs for $X =$ C, N, and O have been investigated using first-principles calculations [1,3,5,20–22]. The obtained results suggest that migration energies of the interstitial solutes tend to increase near a monovacancy. Regarding small pure-vacancy clusters, Fu *et al.* previously showed that they may have either similar or lower migration barriers than the monovacancy in α-Fe, which allowed them to reconcile various experimental observations [23]. Their high mobility is closely linked to their lowest-energy

configurations in a body-centered cubic (bcc) lattice. This result may also be expected for other bcc metals.

Based on the above mentioned features, it is worth investigating whether the fast-migrating vacancy clusters may drag interstitial solutes via a concerted motion. This idea together with the need for a more realistic interpretation of experiments motivated this study, aiming at determining the mobility of interstitial solutes around vacancies, and the migration of small $V_n X_m$ clusters ($n =$ 1–3, and $m =$ 1 or 2) in α-Fe. We perform extensive density functional theory (DFT) calculations for this purpose (Sec. III). In addition, mesoscopic simulations using cluster dynamics (CD) [24] are carried out to explore the impact of the DFT predictions on physical properties, such as the transport of interstitial solutes and the cluster size distributions, of a model Fe system containing vacancies and oxygen atoms (Sec. IV).

II. METHODOLOGY

A. First-principles calculations

First-principles calculations were performed within the DFT framework as implemented in the SIESTA code [25]. They were spin polarized and used the generalized gradient approximation (GGA) with the Perdew-Burke-Ernzerhof (PBE) exchange-correlation functional [26]. Core electrons were replaced by norm-conserving pseudopotentials. Valence electrons were described by linear combinations of numerical pseudoatomic orbitals. The pseudopotential and the basis set for Fe are the same as in Refs. [9,27], with a pseudopotential cut-off radius of 1.15 Å, and a basis set of ten localized functions per atom. The pseudopotentials and basis set for C, N, and O are the same as in Ref. [9]. The cut-off radii for the pseudopotentials of C, N, and O are set to 0.66, 0.60, and 0.60 Å respectively. The basis set of each of these three elements includes two strictly localized functions for the $2s$ states and six for the $2p$ states. The cut-off radii are respectively 2.22 and 2.64 Å for the s and p states of C, and 2.95 and 3.09 Å for both N and O. Five functions for the $3d$ states are also included as polarized orbitals in order to increase angular flexibility. The

---

*Corresponding author: chuchun.fu@cea.fr

charge density is represented on a regular 0.067 Å width grid in the real space.

The Methfessel-Paxton broadening scheme with a 0.3 eV width was used [28]. A cubic supercell of 128 Fe sites with a $3 \times 3 \times 3$ k-point grid was employed for simulations involving monomers (X or V), VX, and VX_2 clusters. We used a 250-atom cell with a $2 \times 2 \times 2$ k-point grid for V_2X and V_3X clusters. A calculation was considered converged with respect to the supercell size and the k-point grid if variations of binding energies [Eq. (1)] and migration barriers were smaller than 0.05 eV.

In all the cases, the configuration of defects was optimized by relaxing the atomic positions keeping the volume of the supercell constant as in the defect-free system (constant-volume approximation). The convergence criterion was set to be 0.04 eV/Å for the residual forces. Binding energy corresponding to clustering reactions, for example $V_nX_m + V_{n'}X_{m'} \rightarrow V_{n+n'}X_{m+m'}$, can be calculated as follows:

$$E^{\mathrm{b}}(V_{n+n'}X_{m+m'}) = E(V_nX_m) + E(V_{n'}X_{m'})$$
$$- E(V_{n+n'}X_{m+m'}) - E_0, \quad (1)$$

where $E(V_{n+n'}X_{m+m'})$, $E(V_nX_m)$, and $E(V_{n'}X_{m'})$ are the energy of the system containing respectively $V_{n+n'}X_{m+m'}$, V_nX_m, and $V_{n'}X_{m'}$ in a Fe bcc lattice, and E_0 denotes the energy of the perfect bcc bulk with N Fe atoms. Here, a positive binding energy means that the clustering reaction is exothermic, that is, the interaction between V_nX_m and $V_{n'}X_{m'}$ is attractive. Migration barriers and paths were calculated using the drag method [29], that is, the atomic positions are constrained to relax in a hyperplane perpendicular to the vector connecting the initial and final positions. This method has shown to provide results with satisfactory precision in iron-based and other solid systems [30–35]. We have performed complementary calculations of some of the most relevant binding [9] and migration energies by fully relaxing the volume and/or shape of the supercells, in order to reach a residual pressure of around 5 kbar. In this way, the error of the migration and binding energies due to the current constant-volume approximation is estimated to be less than 0.10 eV.

If the diffusion path of a cluster involves jumps between various local minima with different barriers, a global migration energy of the cluster along this path can be defined, which is useful for parameterizing mesoscopic models such as the cluster dynamics model described below. This migration energy can be approximated by the highest of the barriers, as explained in Appendix. Here we are neglecting the effect that, in principle, the preexponential factor of a multistep migration path should be different from that if there were a single barrier (Appendix).

The dissociation energy is estimated as the sum of the binding energy between V_nX_m and $V_{n'}X_{m'}$ and the energy barrier of the fastest migrating cluster $V_{n'}X_{m'}$, that is:

$$E^{\mathrm{disso}}(V_{n+n'}X_{m+m'}) = E^{\mathrm{b}}(V_{n+n'}X_{m+m'})$$
$$+ E^{\mathrm{mig}}(V_{n'}X_{m'}). \quad (2)$$

Due to the large amount of configurations considered in this DFT study, we limit ourselves on the calculations of the various energetic quantities. Evaluation of the entropic contributions
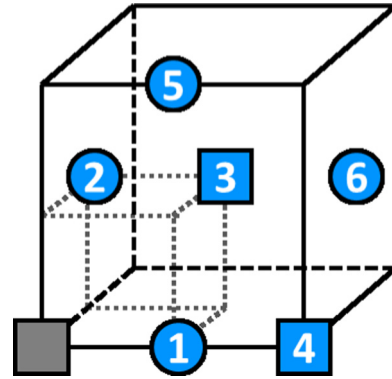

FIG. 1. (Color online) List of nearest-neighbor (nn) sites of an atom sitting on a substitutional site (grey square) of the bcc Fe lattice. Blue circles and squares denote respectively octahedral and substitutional sites. Note that an interstitial solute-vacancy pair can be neither 3 nn nor 4 nn.

are beyond the present scope. Possible consequences and limitations of this approximation for finite temperature discussions will be mentioned in Sec. IV.

For convenience, we want to list the octahedral and the substitutional sites on the same lattice. This is why we split one bcc unit cell into eight simple cubic cells where each vertex corresponds to either a substitutional or an octahedral site. Note that with this notation, a VX pair cannot be third or fourth nearest neighbor. Figure 1 shows the various neighboring sites of one substitutional atom up to the sixth nearest neighbor (nn).

B. Cluster dynamics model

Cluster dynamics (CD) simulations were done with the CRESCENDO code [24]. CD is based on a mean-field formalism and it aims at modeling the evolution of cluster concentrations with time, due to reactions between clusters, interactions of clusters with sinks (e.g., dislocations, grain boundaries) and source terms (e.g., due to irradiation, plastic deformation, mechanical alloying). For mobile clusters ν with neither sinks nor sources considered, CD equations read [24]:

$$\frac{dC_\nu}{dt} = \sum_{\mu \in \mathcal{M}} J_{\nu-\mu,\nu} - \sum_{\mu \in \mathcal{M}} J_{\nu,\nu+\mu} - \sum_{\mu \in \Omega} J_{\mu,\mu+\nu}. \quad (3)$$

For immobile clusters, the last term vanishes. In Eq. (3), $\nu = (n,m)$ is a shorthand for cluster V_nX_m and $\mu = (n',m')$. The set Ω contains all clusters and $\mathcal{M}$ only mobile clusters. C_ν is the concentration of cluster ν. The flux $J_{\nu,\nu+\mu}$ is a net reactive flux between cluster classes ν and $\nu + \mu$ due to the mobility of cluster μ and is given by:

$$J_{\nu,\nu+\mu} = \beta_{\nu,\mu}C_\nu C_\mu - \alpha_{\nu+\mu,\mu}C_{\nu+\mu}, \quad (4)$$

where $\beta_{\nu,\mu}$ and $\alpha_{\nu+\mu,\mu}$ are respectively the absorption and emission rates. Absorption rates are defined by [36]:

$$\beta_{\nu,\mu} = 4\pi(r_\nu + r_\mu)D_\mu. \quad (5)$$

In this equation, D_μ is the diffusion coefficient of cluster μ. This diffusion coefficient can be expressed as $D_\mu = D_\mu^0 \exp[-E^{\mathrm{mig}}(\mu)/kT]$, where D_μ^0 is the diffusion prefactor

and $E^{\mathrm{mig}}(\mu)$ is the migration energy. The distance r_ν is the effective radius of cluster ν and here it is deduced from the atomic volume V_{at} where oxygen atoms and vacancies occupy the same volume for simplicity:

$$\tfrac{4}{3}\pi r_\nu^3 = (n+m)V_{\mathrm{at}}. \qquad (6)$$

Finally, emission rates are given by [37]:

$$\alpha_{\nu+\mu,\mu} = \frac{\beta_{\nu,\mu}}{V_{\mathrm{at}}}\exp\left(-\frac{E^{\mathrm{b}}(\nu+\mu)}{kT}\right), \qquad (7)$$

where $E^{\mathrm{b}}(\nu+\mu)$ corresponds to the binding energy between ν and μ.

III. MOBILITY OF SMALL $V_n X_m$ CLUSTERS FROM FIRST PRINCIPLES

For the three elements (C, N, and O) in a bcc iron lattice, the octahedral site was found to be the lowest-energy solution site in some of our previous work [9], in agreement with other DFT studies [1–3,8,38,39] and experiments [40]. These solute atoms can migrate between octahedral sites through a tetrahedral site. A phonon analysis confirmed that tetrahedral configurations are actually saddle points rather than local minima [41]. The octahedral-tetrahedral energy difference is therefore the energy barrier for the interstitial solute migration. These barriers are respectively 0.85, 0.64, and 0.56 eV for C, N, and O, in good agreement with previous DFT values [1,3,8,20,22] and with existing experimental data for the C case [13]. The energy barrier decreases from C to O, which is consistent with the different nature of solute-Fe interactions [9]. Due to the increase of the $2p$ electronic band filling from C to O, carbon tends to form strong and directional covalent bonds with the neighboring Fe atoms while O-Fe interaction is rather ionic, isotropic, and weaker. Nitrogen shows an intermediate behavior [9]. The energy landscape around C is therefore expected to show more abrupt variations.

Strong attraction between vacancies and interstitial solutes leads to the formation of stable vacancy-solute clusters $V_n X_m$ [1–9]. Once these clusters are formed, several migration mechanisms may take place: (i) cluster diffusion: the cluster migrates without dissociation and its center of mass moves; (ii) cluster dissociation: part of the cluster (generally a monomer X or V) is emitted and then migrates away; (iii) cage movement: for example a solute (X) turns around a vacancy while no translation of center of mass occurs. Note that the two first mechanisms may lead to long-range diffusion of solutes and vacancies forming the cluster, while the cage movement does not. All these mechanisms will be described in this section.
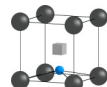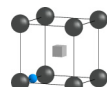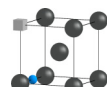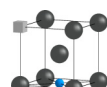
We investigate the mobility of VX and VX_2, which are the dominant clusters at thermal equilibrium [5,6,9], and V_2X and V_3X, which should also emerge under several extreme conditions (plastic deformation, corrosion, irradiation, mechanical alloying, etc.) where abundant vacancies are created.

A. Mobility of VX pairs

1. Diffusion mechanisms

Kinetic properties of the simplest $V_n X_m$ cluster—the VX pair—is investigated for X being C, N, or O. In the

TABLE I. (Color online) Stable and metastable configurations relevant for the VX migration with their respective relative energies (in eV) with respect to the ground state. Cluster binding energies (in eV) of the ground states are given in parentheses. Note that the present binding energies obtained at constant volume are very close to the previous energies calculated at constant pressure [9]. Solute atoms are represented by blue spheres, iron atoms by black spheres, and vacancies by gray cubes.

		C	N	O
1 nn		0 (0.47)	0 (0.78)	0 (1.52)
2 nn		0.58	0.58	0.94
5 nn		0.49	0.77	1.47
6 nn		0.24	0.58	1.17

lowest-energy configuration (the 1 nn configuration represented in Table I), the solute is located between a perfect octahedral site and the vacancy ($\simeq \tfrac{3}{8}a_0$ [001] from the vacancy). X and V are therefore too close to each other in order to jump simultaneously to another equivalent configuration. Therefore, migration paths of VX are piecewise, consisting of successive jumps of either X or V. We have systematically calculated the migration barrier for all the nearest-neighbor solute jumps in the vicinity of the vacancy and the V jumps around the solute in order to find the most favorable paths for the VX migration. All the intermediate metastable configurations involved are presented in Table I. The configurations are labeled in terms of distance between the solute and the vacancy as defined in Fig. 1. Jumps up to the 6 nn configuration are investigated. Both forward and backward jump barriers are given in Table II. Note that some of these barriers have been previously calculated using either first-principles calculations [1,3,20,22] or semiempirical potentials [18]. Our predicted values are in good agreement with the previous ones.

The jump barriers of nitrogen and oxygen atoms near the vacancy are equal to or higher than the barriers for solute diffusion far from the vacancy, if moving from a configuration of lower energy to one of higher energy (1 $nn \to$ 2 nn, 2 $nn \to$ 5 nn, and 6 $nn \to$ 5 nn jumps). On the other hand, the jump barriers of the carbon atom close to a vacancy (1 $nn \to$ 2 nn, 2 $nn \leftrightarrow$ 5 nn, and 5 $nn \leftrightarrow$ 6 nn jumps) are either similar to or much smaller than the interstitial C diffusion barrier far from the vacancy. However, it should be noted that these low-barrier jumps do not necessary lead to a long-range diffusion of the VC pair.

Concerning the vacancy migration near a solute atom, the vacancy bound to a solute generally sees a local barrier equal to or higher than the barrier far from the solute $E^{\mathrm{mig}}(V) = 0.69$ eV, found using the same DFT approach

TABLE II. Energy barriers (in eV) of the solute (vacancy) in the vicinity of the vacancy (solute) relevant to the VX migration, X being C, N, and O.

		C		N		O	
		forward	backward	forward	backward	forward	backward
	$1\,nn \leftrightarrow 1\,nn$	0.50	0.50	0.83	0.83	0.40	0.40
	$1\,nn \leftrightarrow 2\,nn$	0.70	0.11	0.86	0.25	0.94	0.00
Jump of X	$2\,nn \leftrightarrow 5\,nn$	0.66	0.76	0.61	0.41	0.76	0.23
	$5\,nn \leftrightarrow 6\,nn$	0.67	0.92	0.52	0.71	0.43	0.73
	$1\,nn \leftrightarrow 6\,nn$	0.55	0.31	0.74	0.16	1.17	0.00
	$2\,nn \leftrightarrow 5\,nn$	0.67	0.77	0.87	0.67	–	–
Jump of V	$5\,nn \leftrightarrow 6\,nn$	0.63	0.88	0.67	0.86	0.66	0.96

as in Ref. [27]. Similar values (0.60–0.67 eV) have also been reported previously with different DFT implementations [23,42,43]). An exception is the $6\,nn \rightarrow 1\,nn$ barrier, bringing the vacancy back to the solute. Moreover, for the VC pair, the energy barrier for the forward $1\,nn \rightarrow 6\,nn$ jump of vacancy is 0.14 eV lower than the value of 0.69 eV for the free migrating vacancy. Note that the jump of V to go from the $1\,nn$ to the $2\,nn$ is not relevant here: as the solute goes very close to an iron atom, the barrier is likely to be very high, compared to the dissociation energy as estimated in Eq. (2).

Based on the calculated jump barriers, the presence of VX pairs in the solid solutions (at least for $X =$ N and O), are expected to slow down on average the diffusion coefficient of the respective solutes X. Taking into account all possible jumps, one can predict several energetically favorable diffusion paths for VX pairs at their ground-state configuration. Let us consider the case of N in details. Once the VN pair is formed, either the monovacancy or the solute may jump. The barrier for a vacancy to go away from the solute (i.e., $1\,nn \leftrightarrow 6\,nn$) is lower than the jump of the solute atom (i.e., $1\,nn \leftrightarrow 2\,nn$). After this step, it is more favorable that the nitrogen atom jumps, bringing the pair to the $5\,nn$ configuration, where the pair is considered dissociated [$E^{\rm b}(VN, 5\,nn) = 0.01$ eV]. From this state, there are two possibilities as depicted in Fig. 2: (i) the nitrogen atom is trapped again by the vacancy, which induces a translation of the center of mass of the cluster and thus completes the cluster diffusion path; (ii) the nitrogen atom or the vacancy goes away from one another which corresponds to a dissociation path. We have found that the local nitrogen energy barriers to go back toward the vacancy are lower than an isolated nitrogen/vacancy jump barrier in the bulk. As a result, the diffusion path described above may be energetically more favorable (thus more probable) compared to the dissociation jump. Similar multistep migration paths are also found for VC and VO pairs.

If we consider the whole cluster migration path, global migration energies of VX at their ground states can be approximated by the highest barrier of the path (see Appendix). The obtained values are 1.25, 1.29, and 1.90 eV respectively for $X =$ C, N, and O. On the other hand, total dissociation energies [as defined in Eq. (2)] are respectively 1.16, 1.47, and 2.08 eV. The dissociation energy is 0.18 eV higher than the global migration energy for the VN and VO pairs, while it is lower than the VC migration energy. It implies that, within the present approximation where kinetic correlation

effects are not taken into account [44–46] and the difference of preexponential factors of the solute and the vacancy are neglected, the probability that VN and VO pairs migrate as a whole is only slightly higher than the probability of dissociation, and VC pair tends to dissociate rather than migrate.

2. Cage movement

In the simple case of the VX pair, the lowest-energy cage movement consists in the jump of the solute around the vacancy from a nearly octahedral site $1\,nn$ of the vacancy to another one. The saddle point of this single-humped jump is a configuration where the solute is very close to the vacancy (the solute is $\frac{1}{6}a_0$ [101] from the vacancy). Migration barriers are respectively 0.50 eV, 0.83 eV, and 0.40 eV for C, N, and O ($1\,nn \leftrightarrow 1\,nn$ jump in Table II). The cage movement of VN is also possible through the $2\,nn$ configuration. In this case, the barrier is double humped but its value is very close
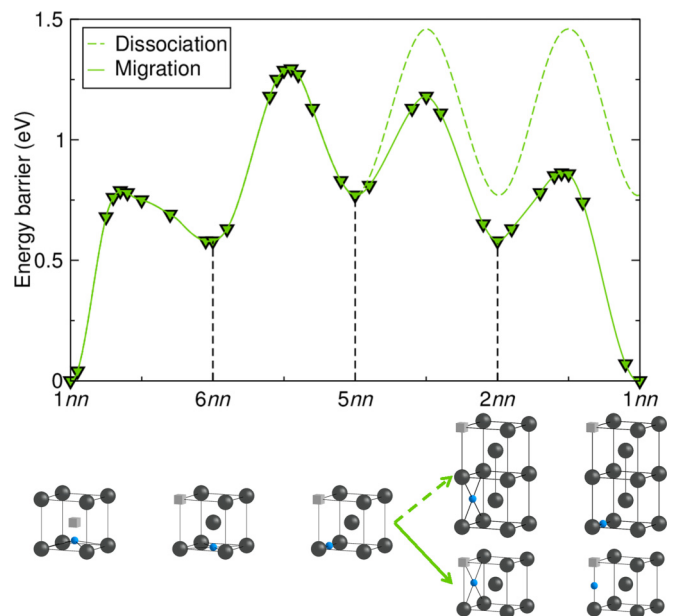

FIG. 2. (Color online) Lowest-energy path found for the diffusion (solid green curve) and the dissociation (dashed green curve) of VN. The stable and metastable configurations are shown in Table I with their respective energies.
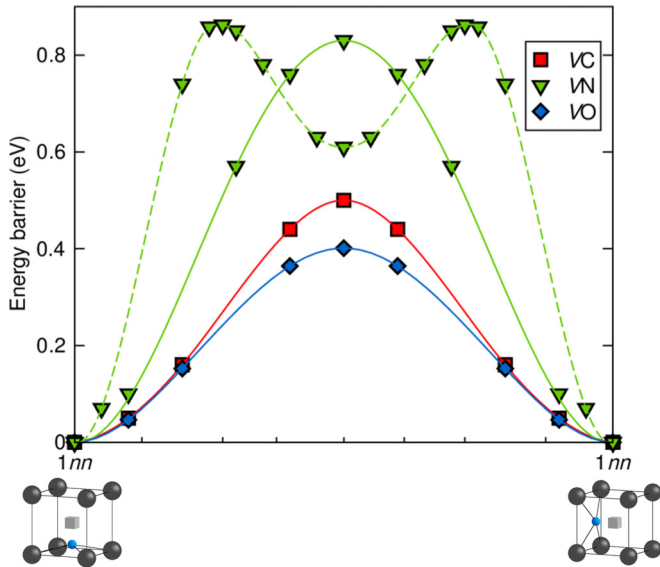
FIG. 3. (Color online) Energy barriers corresponding to the cage movement of VX clusters for $X = C$ (red curve), N (solid and dashed green curves), and O (blue curve). Both one- and two-step paths are shown for the N case.

to the single-humped barrier (the difference is 0.03 eV) and the saddle point configurations are very similar in both cases. Single- and double-humped mechanisms are plotted in Fig. 3. The cage-movement barrier of N around V is higher than the isolated N atom and the VN pair migration barriers. At variance, cage movement barriers of carbon and oxygen atoms are very low compared to the interstitial migration barrier far and in the vicinity of a vacancy described previously. This movement is therefore significantly more probable than the other mechanisms. Once the solute atom is trapped by a vacancy, it may stay a long time turning around the vacancy instead of performing jumps leading to either cluster diffusion or dissociation. Therefore, the cage movements in the C and O cases do not lead to the pair diffusion but are expected to slow down the long-range displacement of the solute. However, this cage movement is neglected in the highest barrier approximation adopted in this paper.

B. Mobility of VX_2

Under thermal equilibrium conditions, VX_2 clusters can be formed in addition to VX pairs [5,6,9]. Moreover, the binding energy for the formation of VX_2 from adding a solute X to VX may be even larger than the binding energy of VX, which makes the VX_2 clusters highly relevant for describing solid solutions at thermal equilibrium. Therefore, diffusion properties of solutes and vacancies may also depend on the diffusion properties of VX_2. The migration of VX_2 clusters for $X = C$, N, and O is studied based on the stable configurations and local minima reported in Table III with their corresponding binding energies.

In the lowest-energy configuration of VX_2, both solute atoms are very close to the vacancy: VC_2 is composed of a strongly bound C_2 dimer besides the vacancy (configuration A in Table III) whereas the two solutes of VN_2 and VO_2

TABLE III. (Color online) Stable and metastable configurations relevant to the VX_2 migration with their respective relative energies (in eV) with respect to the ground state. The binding energies (in eV) corresponding to the addition of X to VX of the ground state are given in parentheses. Solute atoms are represented by blue spheres, iron atoms by black spheres, and vacancies by gray cubes.

		C	N	O
A		0 (0.83)	–	–
B		0.41	0 (0.87)	0 (1.60)
C		0.93	0.60	0.88
D		0.85	0.85	1.54
E		0.68	0.82	1.42
F		0.54	0.86	1.16
G		–	1.04	1.01

are about one lattice parameter from each other (configuration B in Table III). Based on the analysis of VX migration, we predict that VX_2 clusters can diffuse as a whole only through successive and separate jumps of the vacancy and the solutes. Also, high-energy local minima should be generally avoided for the search of favorable cluster migration paths. Therefore, we focus only on intermediate configurations with at least one solute as $1\,nn$ of the vacancy, because X-X interactions far from a vacancy are much lower than V-X interactions [9]. Based on these considerations, one solute has to go far enough (partially dissociates) from the remaining VX to allow migration of the latter. The subsequent jumps of the VX are similar to those described in Sec. III A 1. All the relevant energy barriers involving individual nearest-neighbor jumps of V or X are given in Table IV.

The lowest-energy path found for the diffusion of the three VX_2 clusters is described below. Note that the VC_2 can migrate only if the C_2 dimer splits in order to allow one carbon atom to escape from the vacancy. Once the C_2 dimer breaks up, the energetically most favorable configuration is the configuration B in Table III, which is the ground state of VN_2 and VO_2.

TABLE IV. Energy barriers (in eV) for jumps of either a solute or the vacancy relevant to the VX_2 diffusion for $X =$ C, N, or O.

		C		N		O	
		forward	backward	forward	backward	forward	backward
Jump of X	A ↔ B	0.63	0.21	–	–		–
	B ↔ C	0.83	0.31	0.90	0.31	0.89	0.01
	C ↔ D	0.62	0.70	0.61	0.36	0.84	0.18
	D ↔ E	0.75	0.92	0.64	0.67	0.52	0.63
Jump of V	E ↔ F	0.02	0.15	0.16	0.12	0.01	0.26

From there, the next jumps are identical for the three clusters as shown in Fig. 4. First, one solute jumps step by step, leaving the vacancy (from configuration B to E). During these jumps, the interaction between the two solutes remains small [9]. Thus, migration mechanisms of X in the vicinity of VX are very similar to the migration of X around V as studied in the previous section. Most of the energy barriers are consequently similar between the VX and the VX_2 cases. The small differences may be due to the residual interactions between the two solutes during the migration. Starting from configuration D, the first solute is dissociated from the VX pair, in terms of the X-to-VX binding energies. From there, as described in the VX subsection, two mechanisms may occur: (i) the first solute atom goes farther from the vacancy, which then follows it. To complete the diffusion path, the second solute has to reach the newly formed VX pair in a symmetric way. (ii) the solute atom continues escaping from the vacancy leading to the complete dissociation of the cluster. VX_2 dissociation barriers are respectively 1.68, 1.51, and 2.16 eV for C, N, and O while the corresponding global migration barriers for the clusters at their ground states are 1.60, 1.48, and 2.06 eV. The dissociation energy is about 0.10 eV larger than the corresponding global migration energy for VC_2 and VO_2, while for VN_2, they are similar. Overall, the VX and VX_2 clusters are not expected to

diffuse over large distances without dissociation, but they may diffuse by successive dissociations and reassociations.

Concerning the cage movements, rigid rotation of the C_2 dimer around the vacancy in VC_2 passes through energetically degenerate states as depicted in Fig. 5(a). The energy difference between these states is around 0.03 eV, lower than the uncertainty limit of the calculations. Since the energy landscape is very flat, jumps between them are practically athermal (migration barriers are almost zero). In contrast, solutes turning around the vacancy in VN_2 and VO_2 require significantly higher barriers [Fig. 5(b)].

C. Mobility of V_2X and V_3X

Under extreme conditions (plastic deformation, corrosion, irradiation, mechanical alloying etc.), when abundant vacancies are created, clusters composed by multiple vacancies
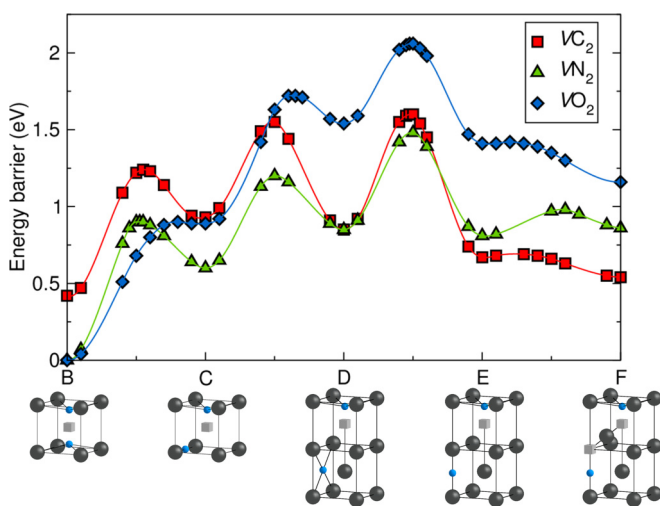
(a)

FIG. 4. (Color online) The first half of the lowest-energy migration path found for VX_2 with $X =$ C (red curve), N (green curve), and O (blue curve). The second half of the path (not shown) is symmetric (F → B) to the shown part of the path. All the metastable states are shown in Table III with their respective energies.
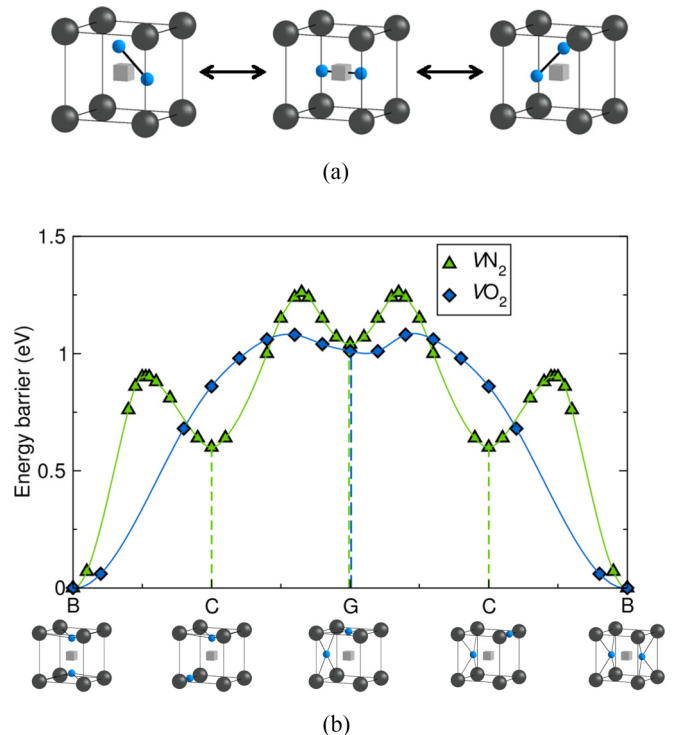
(b)

FIG. 5. (Color online) (a) Stable and metastable configurations involved in the cage movement of VC_2 where the jump barriers are all negligible. Solute atoms are represented by blue spheres, iron atoms by black spheres, and vacancies by gray cubes. (b) Energy barriers for the cage movement of VN_2 and VO_2.
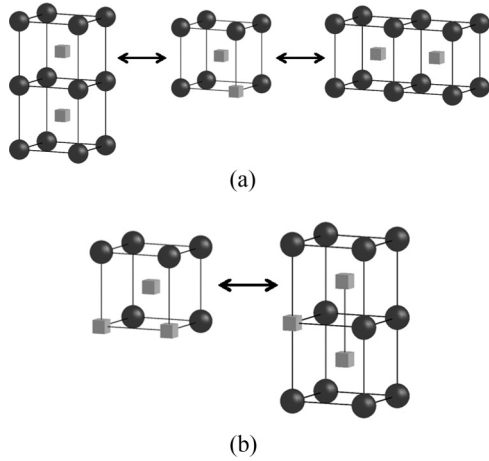
(a)

(b)

FIG. 6. Migration path of (a) V_2 and (b) V_3 in bcc iron [23]. The global migration energies are respectively 0.70 eV and 0.25 eV [27]. Iron atoms are represented by black spheres and vacancies by gray cubes.

and one interstitial solute are very likely to form in the solid solution. In addition, a low-energy barrier was previously obtained for the diffusion of divacancy and trivacancy clusters (respectively 0.70 eV and 0.25 eV compared to 0.69 eV for the monovacancy), and of the trivacancy containing one hydrogen atom [27] in α-Fe. We investigate if there is a similar behavior for these vacancy clusters containing a carbon, a nitrogen or an oxygen atom.

1. V_2X migration

The lowest-energy state of V_2 in bcc iron consists in two vacancies separated by one lattice parameter along a (100) direction, and its migration requires two consecutive nearest-neighbor jumps of a vacancy to move from a ground-state configuration to another one [23] [Fig. 6(a)]. The lowest-energy configuration of V_2X is similar to that of V_2, and identical for the three elements, with the solute at the 1 *nn* site of both vacancies (configuration H in Table V). Therefore, in the presence of a solute atom, vacancies may perform the same jumps as in V_2, followed by rearrangement jumps of the solute, leading to the diffusion of the whole cluster. The vacancy jump barriers depend naturally on the position of the solute. All involved forward and backward migration barriers are given in Table VI. Starting from the lowest-energy configuration (configuration H), either the solute (H $\leftrightarrow$ I) or a vacancy plus the solute (H $\leftrightarrow$ J) may jump, that is, either the solute moves first to facilitate the subsequent vacancy jump, or one vacancy and the solute jump simultaneously. The energy barrier for the first mechanism is as expected much lower for the three cases. The whole diffusion path consists actually in consecutive and alternative jumps of the solute and a vacancy, as depicted in Fig. 7. Note that at variance with the previous clusters studied (VX and VX_2), the vacancy or the solute are always bound to the rest of the cluster during the cluster migration. The global migration energies of V_2X clusters along the above described path are 1.05, 1.05, and 1.27 eV respectively for the C, N, and O case. They are all lower than the migration energies of the corresponding VX and VX_2 clusters. The lowest-energy path

TABLE V. (Color online) Stable and metastable configurations relevant to V_2X migration, for $X =$ C, N, and O, with their respective relative energies with respect to the ground states (in eV). The binding energies (in eV) corresponding to the addition of V to VX of the ground state are given in parentheses. Solute atoms are represented by blue spheres, iron atoms by black spheres, and vacancies by gray cubes.

		C	N	O
H		0.00 (0.48)	0.00 (0.49)	0.00 (0.82)
I		0.21	0.25	0.53
J		0.67	0.46	0.47
K		0.24	0.28	0.63

for the complete dissociation of V_2X clusters consisting in one of the vacancies leaving the cluster. The corresponding energy barriers are 1.17, 1.18, and 1.51 eV respectively for C, N, and O, which are all at least 0.12 eV higher than the corresponding cluster migration barriers. Cluster migration as a whole may therefore be more probable than dissociation.

2. V_3X migration

It is particularly interesting to investigate the diffusion of V_3X clusters, as V_3 clusters diffuse much faster than the monovacancies and other vacancy clusters. The obtained migration energies for V_3 and V are respectively 0.25 eV and 0.69 eV. Indeed, V_3 is the smallest vacancy cluster able to keep continuously its ground-state configuration while migrating. Its migration consists in successive nearest-neighbor jumps of individual vacancies [23] [Fig. 6(b)].

The lowest-energy configuration of V_3C and V_3N is different from that of V_3O: for C and N, the solute is 1 *nn* of one vacancy but far from (6 *nn*) the other two vacancies (configuration L in Table VII) whereas for O, the solute tends to be close to all three vacancies (configuration P in Table VII). This difference is indeed consistent with the weaker Fe-O interaction and larger effective volume of O in bcc iron [9]. Also note that V_3O has an energetically degenerate configuration (configuration S in Table VII) where the trivacancy cluster configuration is less compact: the three vacancies are lying within a {001} plane.

Therefore, for C and N, the lowest-energy diffusion path of V_3C and V_3N is composed of nearest-neighbor jumps of individual vacancies (the same as for V_3 migration), followed by jumps of the solute for recovering its favorable position

TABLE VI. Energy barriers (in eV) relevant to the V_2X diffusion for $X = $ C, N, and O. The stable and metastable states are shown in Table V.

		C		N		O	
		forward	backward	forward	backward	forward	backward
Jump of X	H $\leftrightarrow$ I	0.61	0.40	0.83	0.58	0.65	0.12
	J $\leftrightarrow$ K	0.14	0.57	0.55	0.73	0.40	0.24
Jump of V	H $\leftrightarrow$ J	1.34	0.67	1.42	0.96	1.34	0.87
	I $\leftrightarrow$ J	0.84	0.38	0.80	0.59	0.62	0.68
	K $\leftrightarrow$ I	0.55	0.58	0.63	0.66	0.64	0.74

[Fig. 8(a)]. For V_3O, the oxygen atom first needs to go out from the divacancy to allow the trivacancy cluster migration. Then, the successive steps are similar to the case of V_3C and V_3N [Fig. 8(b)]. Regarding the migration of the degenerate less compact V_3O configuration, the farthest vacancy has to jump to reach the compact ground state (the P configuration) and then the cluster can migrate as previously described.

In the three cases, the solute atom always stays as 1 *nn* of at least one vacancy during the migration, and V_3X clusters remain strongly bound during the diffusion, more than V_2X clusters. Therefore, all the barriers involved in the cluster diffusion path are rather low (Table VIII), leading to global migration energies of 0.59, 0.86, and 0.58 eV respectively for V_3C, V_3N, and V_3O. Comparing the global migration barriers, V_3X are systematically more mobile than the above described VX, VX_2, and V_2X for all the three solutes. Concerning the cluster dissociation, the most probable path for the case of N and O, where vacancy-solute binding energies are high, consists in the emission of a vacancy. The resulting dissociation energies are 0.98 and 0.95 eV respectively for V_3N and V_3O. For the carbon case however, it is energetically more favorable that the solute atom escapes from the trivacancy with a dissociation energy of 0.97 eV (and a corresponding binding energy of 0.72 eV). For C and O cases, the dissociation energies are significantly higher than the cluster diffusion energies, making long-range diffusion of V_3X highly probable without dissociation.
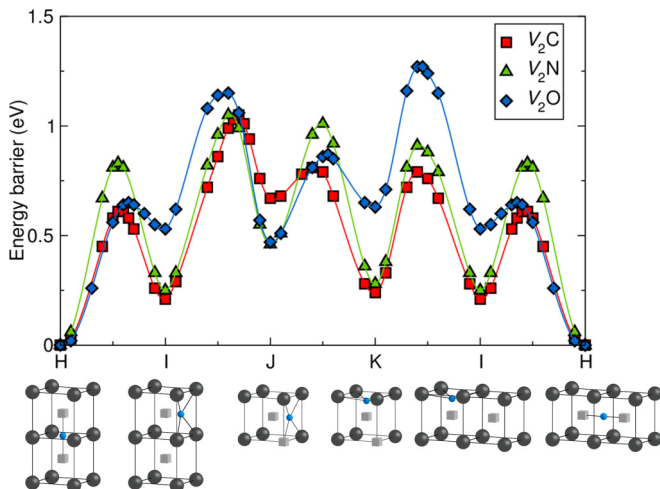
Figure 9 summarizes the global migration barriers of the vacancy-solute clusters at their respective ground states, based on the lowest-energy paths found. It reveals that the three

TABLE VII. (Color online) Stable and metastable configurations relevant to the V_3X migration for $X = $ C, N, and O with their respective relative energies with respect to the ground state (in eV). The binding energies (in eV) corresponding to the addition of V to V_2X of the ground state are given in parentheses. Solute atoms are represented by blue spheres, iron atoms by black spheres, and vacancies by gray cubes.

		C	N	O
L		0.00 (0.37)	0.00 (0.29)	–
M		0.13	0.13	–
N		0.49	0.22	–
O		0.38	–	0.38
P		–	–	0.00 (0.26)
Q		–	–	0.20
R		–	–	0.18
S		–	–	0.01

FIG. 7. (Color online) Lowest-energy diffusion path found for V_2X cluster with $X = $ C (red curve), N (green curve), and O (blue curve). The stable and metastable states are shown in Table V with their respective energies.

TABLE VIII. Energy barriers (in eV) involved in the V_3X migration for $X =$ C, N, or O. All the metastable configurations are shown in Table VII.

		C		N		O	
		forward	backward	forward	backward	forward	backward
Jump of X	M ↔ N	0.39	0.05	0.73	0.64	–	–
	N ↔ L	0.10	0.59	0.51	0.73	–	–
	P ↔ Q	–	–	–	–	0.44	0.24
	R ↔ P	–	–	–	–	0.27	0.45
Jump of V	L ↔ M	0.36	0.23	0.41	0.28	–	–
	Q ↔ R	–	–	–	–	0.33	0.35
	P ↔ S	–	–	–	–	0.69	0.68

solutes exhibit a similar kinetic behavior in the presence of vacancies; VX and VX_2 clusters are significantly less mobile than the isolated solutes X, while V_2X and V_3X clusters
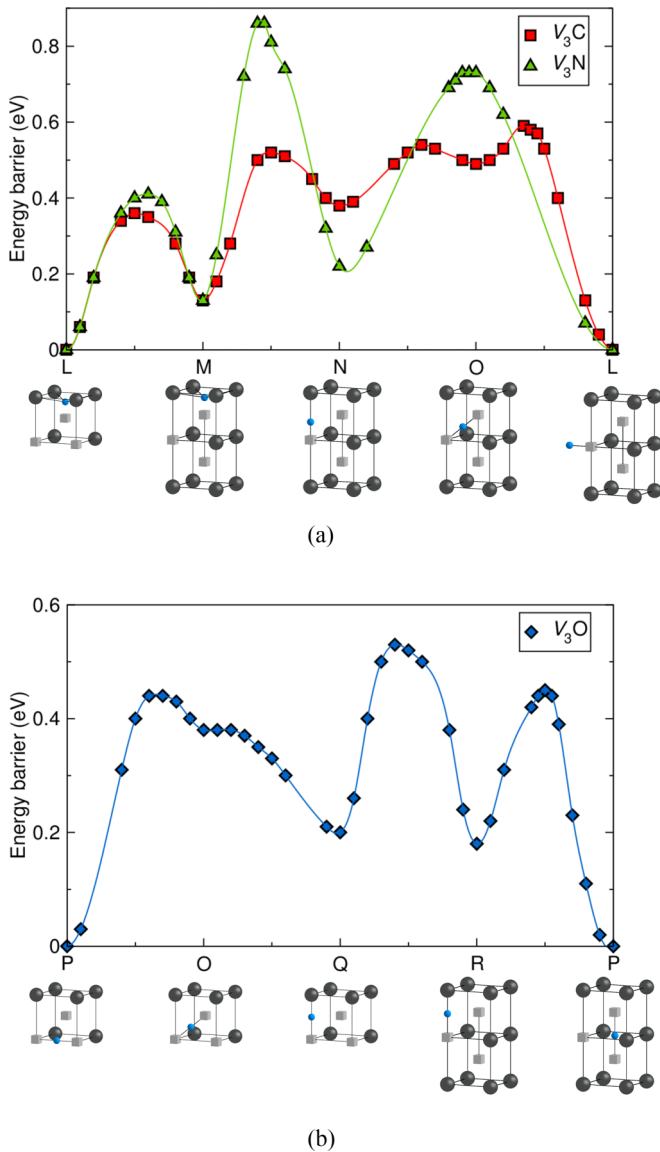

(a)

(b)

FIG. 8. (Color online) Lowest-energy diffusion path found for (a) V_3C (red curve) and V_3N (green curve) and for (b) V_3O cluster. All the metastable configurations are shown in Table VII with their respective energies.

are overall more mobile, compared with the VX and VX_2. Indeed, if comparing the global barriers, V_3X appears to be systematically the most mobile cluster. Very interestingly, V_3O may be as mobile as the octahedral O atom, and V_3C may be even more mobile than an isolated C atom. The high mobility of these clusters suggests that, in contrast to common beliefs, the mobility of interstitial atoms is not necessarily lower once they get trapped by vacancies. Effective diffusion coefficients of the solute species may also be affected by the presence of these clusters. In addition, the very mobile vacancy-solute clusters may drag the solutes towards sinks such as dislocations and grain boundaries. In this way, they may modify the segregation profile of the solutes at sinks. Further studies analyzing the coupling of vacancy and solute fluxes [44–46] are required to gain more insights, which are beyond the scope of the present work.

The low migration barriers of V_3X are strongly linked to the high mobility of the trivacancy in a bcc lattice, which should be due to geometrical reasons. Here we perform complementary DFT calculations to verify another bcc metal: niobium (Nb). For a more accurate inclusion of semicore states ($4p$), the VASP implementation of DFT is used [47–49] using the projector augmented wave (PAW) method, and plane-wave basis sets with a cutoff of 400 eV. The other approximations are the same as described in Sec. II A. As expected, the trivacancy in Nb is also very mobile, its migration energy is 0.32 eV, compared
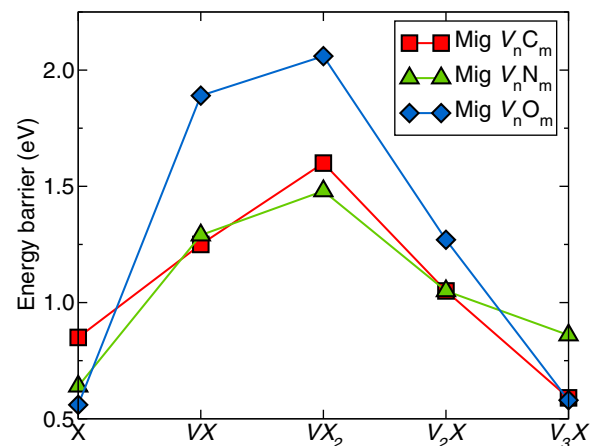

FIG. 9. (Color online) Global migration energies of V_nC_m (squares), V_nN_m (triangles), and V_nO_m (diamonds) from one ground-state configuration to another.

with 0.53 eV for the monovacancy. Therefore, the mobility behavior of V_3X found may also be expected for various interstitial solutes and in other bcc metals, providing that the cluster is stable enough against dissociation. Previously, Hayward and Fu have shown that it is indeed the case of a trivacancy containing a H atom [27].

V_nX_m cluster mobilities may have visible effects on the solute properties only if a significant amount of them is present in the material. In order to combine the mobility properties of clusters predicted by DFT and their concentrations under given conditions, we perform complementary cluster dynamics simulations (Sec. IV). Also, it allows us to account for the interactions (agglomeration, dissociation) between a large number of vacancy-solute clusters.

IV. IMPACT OF SMALL MOBILE CLUSTERS BY CD SIMULATIONS

In this study, we perform CD simulations for the oxygen case only, since a qualitatively similar behavior is expected for carbon and nitrogen. Indeed, these three solutes have similar kinetic properties, as described in the previous section. Furthermore, we expect O to be more impacted by V than C and N as its interaction with V is the strongest among the three elements [3,9,20].

The parameters of our model rely on DFT calculations for small clusters. For pure vacancy clusters containing up to six vacancies, binding and migration energies have been calculated previously and given in Refs. [23,27]. Formation and binding energies of small clusters (up to four vacancies and four solutes) are given by our previous DFT study [9]. Energetics of larger clusters (up to $n + m = 100$) are determined using a lattice interaction model based on DFT data developed in Ref. [9]. This set of cluster configurations has been obtained using a configurational space exploration method also described in Ref. [9]. For simplicity, in our CD simulations, we take into account only the ground states found. The present DFT results, shown above, are used as input data for migration energies of small V_nO_m clusters. We perform simulations for temperatures ranging from 300–600 K. We assume that all the diffusion coefficients have the same prefactor D_μ^0 as for the monovacancy ($8.2 \times 10^{-7} \mathrm{m}^2\mathrm{s}^{-1}$ [24]). Based on our DFT study, we know that all the cluster migration and dissociation occur by successive jumps of either a single solute or a single vacancy. Experimental data showed that the diffusion prefactor for carbon (the lightest of the three solutes) in iron is around 6.2×10^{-7} to $1.7 \times 10^{-7}\mathrm{m}^2\mathrm{s}^{-1}$ (Refs. [50,51]) and for oxygen is estimated to $1 \times 10^{-6}\mathrm{m}^2\mathrm{s}^{-1}$ (Ref. [52]), which are not significantly far from the adopted prefactor for the monovacancy. We therefore consider that assuming the same prefactor for all the clusters should be an acceptable approximation. Indeed, at 600 K, the difference of prefactor of a factor 5 is equivalent to a difference of migration energy of less than 0.10 eV (see also Appendix).

To highlight the role of small mobile clusters, two different sets of parameters for migration energies are used. In the first case, only O monomers and small V_n clusters are mobile (parametrization 1): $\mathcal{M}_1 = \{O, V_{n \leqslant 6}\}$. In the second case, small V_nO_m clusters can also migrate (parametrization 2): $\mathcal{M}_2 = \{O, V_{n \leqslant 6}, VO, V_2O, V_3O, VO_2\}$.
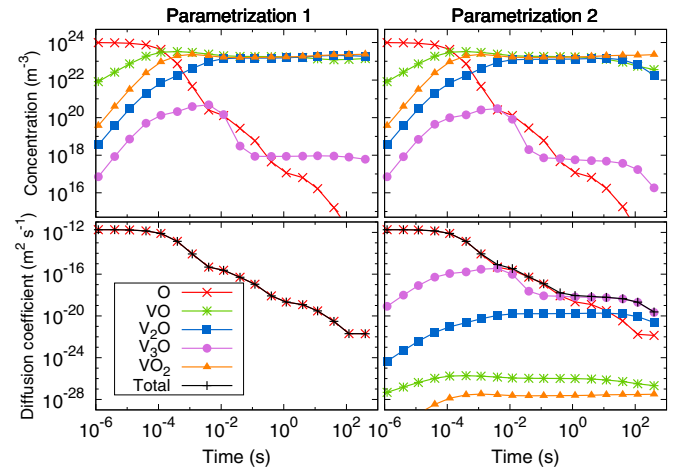

FIG. 10. (Color online) Evolution of concentration of small mobile V_nO_m clusters (top) and contribution of each species to the effective diffusion coefficient of oxygen (bottom) with parametrization 1, where only the O monomers are mobile (left) and with parametrization 2, where small V_nO_m clusters are mobile (right). The calculations are performed at 500 K.

We consider a model case where the iron system contains initially only V and O monomers with concentrations equal to $10^{24}\mathrm{m}^{-3}$. This oxygen concentration is very large compared to its low solubility limit in iron, for all the temperatures considered in this study [9]. The vacancies are also in excess compared to the thermal equilibrium. Sources and sinks for point defects and solutes are not considered.

First, we investigate the evolution of small mobile clusters with time to highlight their role on oxygen transport. Evolutions are similar for all temperatures considered and we thus only represent the results for $T = 500$ K in Fig. 10. For both parametrizations, cluster concentrations are shown to increase and then decrease or level off. The VO, VO_2, and V_3O concentrations sharply drop at around $t = 10^{-1}$s and $t = 10^{-2}$s respectively for parametrization 1 and 2. For parametrization 2, a second drop is clearly seen at times greater than 10^2 s for V_3O, V_2O, and VO.

Looking into more detail at the evolution of concentrations with time, it appears that the initial increase of V_nO_m concentration is due to the migration of V, V_2, and V_3. At around $t = 10^{-4}$s, there is more dissociation of VO and VO_2 clusters than formation because of the depletion of V concentration due to the formation of larger clusters. As a consequence, after reaching the maximum of their concentrations at $t = 10^{-4}$s, both VO and VO_2 cluster concentrations decrease to the same concentration as V_2O at $t = 10^{-2}$s. Mechanisms of disappearance of V_3O are not the same with parametrizations 1 and 2. An analysis of fluxes [i.e., creation and loss terms in Eq. (4)] shows that with parametrization 1, V_3O concentration decreases essentially due to the dissociation of V_3O. With parametrization 2, the disappearance of V_3O is explained not only by its dissociation, but also by its agglomeration with other V_nO_m clusters due to its migration. This additional elimination term explains why the decrease of V_3O occurs earlier when migration of small clusters is enabled. The higher the temperature, the larger the ratio of the dissociation flux to

the migration flux of V_3O. Indeed, it is directly proportional to $\exp[-(E^{\text{disso}}(V_3\text{O}) - E^{\text{mig}}(V_3\text{O}))/kT]$, with $E^{\text{disso}}(V_3\text{O}) > E^{\text{mig}}(V_3\text{O})$.

A second drop is visible for parametrization 2 at around 100 s for VO, V_2O, and V_3O. The decrease of VO and V_2O is simply explained by the fact that with this parametrization, larger clusters are formed. These clusters are more stable and produce less VO, V_2O, and V by dissociation. Two factors explain the depletion of V_3O. First, the smaller concentrations in V, VO, and V_2O lead to smaller creation rate of V_3O. Secondly, the mobility of V_3O is responsible for its absorption by larger clusters.

The contribution of vacancies to O transport can be determined more quantitatively by defining an effective diffusion coefficient as follows:

$$D^{\text{eff}}(\text{O}) = \sum_{\mu \in \mathcal{M}_{i=1,2}} D_\mu \frac{C_\mu}{C_{\text{O}}^{\text{tot}}}, \tag{8}$$

where $C_{\text{O}}^{\text{tot}}$ is the global concentration of O. Here again we focus on the simulations at 500 K (Fig. 10). With parametrization 1 the effective diffusion coefficient simply reduces to the diffusion coefficient of O monomer. If small clusters are mobile (parametrization 2), the evolution of $D^{\text{eff}}(\text{O})$ closely follows the evolution of O concentration up to a time when the concentration of V_3O becomes larger than the concentration of O. Since the migration energies of these two species are nearly the same, the contribution of V_3O cannot be neglected from this time. We emphasize here that although the concentrations of V_2O and VO are orders of magnitude larger than V_3O, they do not have any effect on the migration of O due to their low mobility.

Since solute transport can be modified by the mobility of small clusters, it is interesting to investigate whether cluster distributions are also altered by this mobility. In Fig. 11 we show the cluster distributions at 500 K obtained with parametrizations 1 and 2. At short times [Figs. 11(a) and 11(b)], the distributions are similar with both parametrizations. Indeed, during this stage, the same mechanisms are responsible for cluster evolution, that is, the migration of V, V_2, V_3, and O. For longer times [Figs. 11(c)–11(f)], the cluster distributions are different: larger clusters are formed when all the mobile clusters are included in the calculations. Actually, we have checked that enabling only the V_3O mobility allows us to fully account for these changes in cluster distributions. We therefore confirm that it is essentially the migration of V_3O that accelerates the formation of larger clusters. It is thus shown that even if V_3O concentration is low, its effect on cluster distributions and more generally on the microstructure cannot be neglected.

We have tested the validity of our conclusions regarding the effect of cluster configurational entropy. The configurational space exploration method coupled with the lattice interaction model used to determine the most stable configuration of each cluster and their formation energy was also employed to obtain the configuration and the formation energy for metastable states for each cluster along with their geometrical multiplicity [9]. We have estimated the free formation energy for each $V_n\text{O}_m$ cluster taking into account the contribution of the configurational entropy for stable and metastable states.
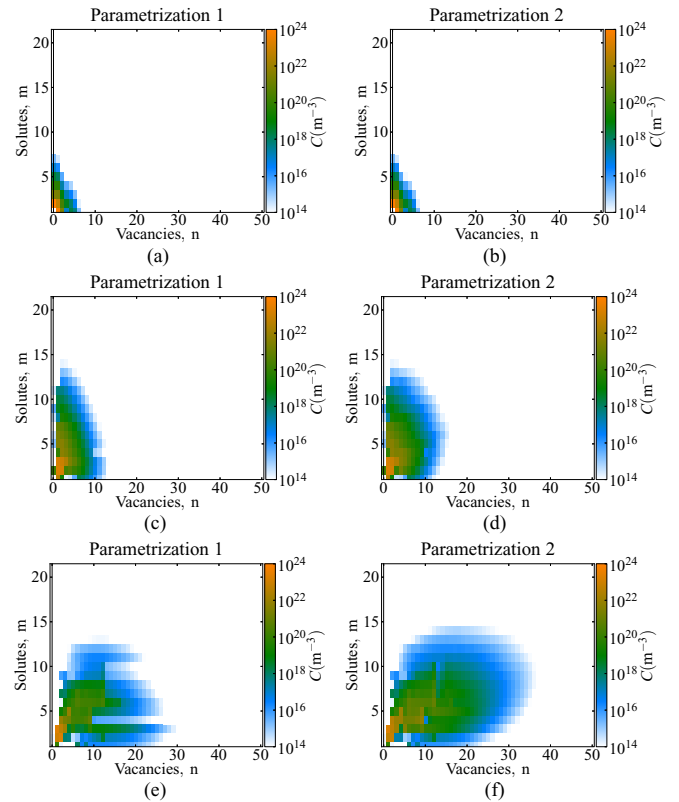

FIG. 11. (Color online) Cluster distributions at 500 K with parametrization 1, when only O and $V_{n \leqslant 6}$ clusters are mobile (left plots) and with parametrization 2, when small mobile $V_n\text{O}_m$ clusters are taken into account (right plots) (a) and (b) at 10^{-5} s, (c) and (d) at 10^{-2} s, and, (e) and (f) at 100 s.

Additional cluster dynamics simulations have been performed with this new parametrization at 600 K, at which entropy effects are the highest. The same results have been obtained concerning the impact of the small mobile clusters: they may increase the diffusion coefficient of oxygen and promote the formation of larger clusters. It is worth noting that the next higher-energy configurations of the mobile clusters show an energy difference of 0.94, 0.88, and 0.47 eV respectively for VO, VO$_2$, V_2O. For V_3O cluster, there exists a degenerate configuration and the next higher-energy configuration exhibits a difference of 0.18 eV. As discussed in Sec. III C 2, effective migration barriers are practically the same for the two degenerate configurations. Therefore, it is reasonable to neglect migration paths for the metastable clusters for the temperature range considered (300–600 K).

Above, we have reported a detailed analysis for a given concentration of oxygen and vacancy. Additionally, we have also performed CD simulations for various O concentrations and vacancy-to-oxygen ratios, within the 300–600 K temperature window. The obtained results show that V_3O may have an impact on the O diffusion during a significant range of time if the total concentration of vacancies is equal or greater than to the total concentration of O, even at very low O concentrations (10^{21}m^{-3}). Therefore, the present conclusion should apply if the system contains a supersaturation of vacancies, created by

processes such as irradiation, corrosion, plastic deformation, or mechanical alloying.

V. CONCLUSIONS

A systematic density functional theory study has been performed to determine energy barriers for jumps of an interstitial solute around a vacancy or a vacancy cluster, and of a vacancy near a solute in bcc iron. Based on these data, energetically favorable migration mechanisms have been predicted for small $V_n X_m$ clusters ($n = 1$–3, and $m = 1$ or 2) with $X =$ C, N, and O, which are the most common interstitial solutes in iron and in many other transition metals. The three solutes exhibit similar diffusion characteristics, that is, VX and VX_2, which are the dominant clusters at thermal equilibrium, show very low mobility (without complete dissociation). Based on our results, the solute monomers are essentially the only species responsible for the mobility of the solutes in equilibrium conditions. On the other side, $V_2 X$ and $V_3 X$ clusters are found to be overall more mobile. In particular, by comparing global migration energies, $V_3 X$ is systematically the most mobile cluster for $X =$ C, N, and O, as well as for $X =$ H, studied previously [27]. This common feature relies on the high mobility of the compact trivacancy in a bcc lattice. Additional calculations were performed and have confirmed the large mobility of V_3 in bcc niobium. Interstitial solutes can follow the motion of the trivacancy through successive jumps while staying bound to at least one of the vacancies. As a consequence, the high mobility of $V_3 X$ may be expected for a large variety of interstitial solutes in any bcc metal, providing that such cluster is sufficiently stable against dissociation.

In the present case of iron, we find that, very interestingly, $V_3 O$ may be as mobile as the octahedral oxygen, and $V_3 C$ may be even more mobile than an isolated C atom. Therefore, at variance with common beliefs, trapping of interstitial solutes by vacancies does not necessarily reduce their mobility. Parametrized on energetics and mobility of $V_n O_m$ clusters (with $n + m$ up to 100) from DFT or an atomic-interaction model, cluster dynamics simulations are performed assuming a simple iron system. The goal was to investigate the impact of small mobile vacancy-solute clusters on properties such as the transport of oxygen and the cluster size distributions, in the presence of a supersaturation of vacancies, created by processes such as irradiation, plastic deformation, corrosion, mechanical alloying, etc. The presence of the highly mobile clusters is shown to increase the effective diffusion coefficient of the solute in some conditions. In addition, it promotes the formation of large-size clusters. Therefore, the mobility of the small vacancy-solute clusters cannot be neglected for understanding and interpreting experimental data, especially when considering materials under extreme conditions.

ACKNOWLEDGMENTS

APPENDIX: DETERMINATION OF THE GLOBAL MIGRATION ENERGY OF A MULTISTEP MIGRATION PATH

In this section, we demonstrate that taking the highest barrier of a multistep diffusion path as the global barrier migration is a reasonable approximation. Let us consider the diffusion path described in Fig. 12 as the most favorable among all paths considered.

We define the jump frequency of the whole diffusion path as:

$$\Gamma = \Gamma_0 \exp\left(-\frac{E^{\mathrm{mig}}}{kT}\right). \tag{A1}$$

Two trajectories are compared: going from Z_1 to Z_2 and from Z_1 to Z_1 through Y. The rate of the element to go from Z_1 to Z_2 along this path is the rate of passing the first barrier and then the second without going back to Z_1, which corresponds to the following rate:

$$\Gamma = \Gamma_1 \frac{\Gamma'_2}{\Gamma'_1 + \Gamma'_2}. \tag{A2}$$

If the energy barrier to go back from Y to Z_1 is smaller than the barrier to go to Z_2, Eq. (A2) can also be written as follows:

$$\Gamma = \alpha \frac{\Gamma_1 \Gamma'_2}{\Gamma'_1}, \quad \text{where} \quad \alpha = \frac{1}{1 + \frac{\Gamma'_{0,2}}{\Gamma'_{0,1}} \exp\left(-\frac{E'_2 - E'_1}{kT}\right)}. \tag{A3}$$

As $E'_1 \leqslant E'_2$, whatever the precise value of $E'_2 - E'_1$, the α term is comprised between $\frac{1}{1 + \frac{\Gamma'_{0,2}}{\Gamma'_{0,1}}}$ and 1 which can be approximated as a modification of the diffusion prefactor only. Therefore, the major evolution with temperature of Γ is due to the other
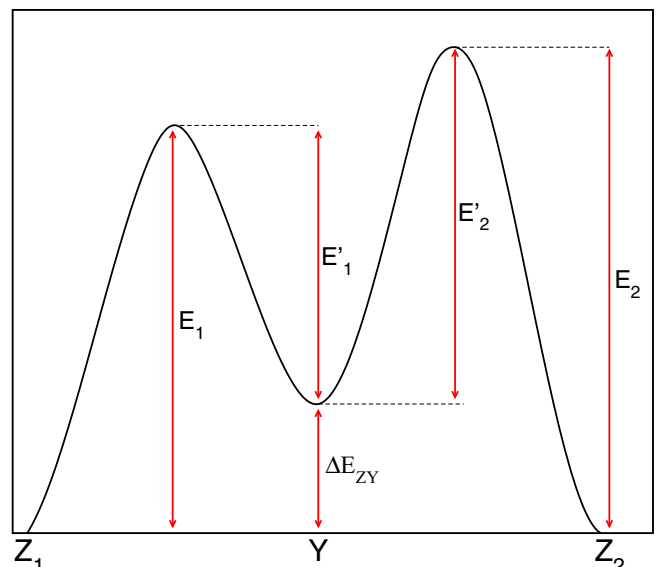

FIG. 12. (Color online) Example of diffusion path.

term, so that it can be written:

$$\Gamma \simeq \Gamma_0 \exp\left(-\frac{E_1 + E_2' - E_1'}{kT}\right). \tag{A4}$$

As $E_1 = E_1' + \Delta E_{ZY}$,

$$E^{\mathrm{mig}} \simeq E_2' + \Delta E_{ZY} = E_2, \tag{A5}$$

which shows that the global energy barrier corresponds to the highest barrier.

Conversely, if $E_1' \geqslant E_2'$, then we obtain similarly that:

$$\Gamma = \frac{\Gamma_1}{1 + \frac{\Gamma_{0,1}'}{\Gamma_{0,2}'} \exp\left(-\frac{E_1' - E_2'}{kT}\right)}. \tag{A6}$$

The same argument as before holds, and we obtain in this case that, within a reasonable approximation:

$$E^{\mathrm{mig}} \simeq E_1. \tag{A7}$$

In conclusion, we show that the global energy barrier is approximately equal to the highest barrier, i.e., the difference between the ground-state energy and the highest saddle point energy. Note that the preexponential factor for a multijump path should be reduced compared to a single-jump path. We have estimated such reduction for the most relevant case of the V_3O cluster migration to be less than a factor 5 up to 600 K, the highest temperature considered in the present study. At 600 K, a reduction of factor 5 in the prefactor is equivalent to an increase of global energy barrier of around 0.08 eV.

[1] C. Domain, C. S. Becquart, and J. Foct, Phys. Rev. B **69**, 144112 (2004).
[2] C. J. Först, J. Slycke, K. J. Van Vliet, and S. Yip, Phys. Rev. Lett. **96**, 175501 (2006).
[3] C. L. Fu, M. Krcmar, G. S. Painter, and X.-Q. Chen, Phys. Rev. Lett. **99**, 225502 (2007).
[4] T. Ohnuma, N. Soneda, and M. Iwasawa, Acta Mater. **57**, 5947 (2009).
[5] C.-C. Fu, E. Meslin, A. Barbu, F. Willaime, and V. Oison, Solid State Phenom. **139**, 157 (2008).
[6] T. Jourdan, C.-C. Fu, L. Joly, J. Bocquet, M. Caturla, and F. Willaime, Phys. Scr., T **145**, 014049 (2011).
[7] A. T. Paxton and C. Elsässer, Phys. Rev. B **87**, 224110 (2013).
[8] A. Claisse and P. Olsson, Nucl. Instrum. Methods Phys. Res., Sect. B **303**, 18 (2013).
[9] C. Barouh, T. Schuler, C.-C. Fu, and M. Nastar, Phys. Rev. B **90**, 054112 (2014).
[10] V. Irmer and M. Feller-Kniepmeier, Philos. Mag. **25**, 1345 (1972).
[11] L. De Schepper, D. Segers, L. Dorikensvanpraet, M. Dorikens, G. Knuyt, L. Stals, and P. Moser, Phys. Rev. B **27**, 5257 (1983).
[12] A. Vehanen, P. Hautojärvi, J. Johansson, J. Yli-Kauppila, and P. Moser, Phys. Rev. B **25**, 762 (1982).
[13] S. Takaki, J. Fuss, H. Kuglers, U. Dedek, and H. Schultz, Radiat. Eff. **79**, 87 (1983).
[14] H. Wagenblast and A. Damask, J. Phys. Chem. Solids **23**, 221 (1962).
[15] F. Fujita and A. Damask, Acta Metall. **12**, 331 (1964).
[16] R. Arndt and A. Damask, Acta Metall. **12**, 341 (1964).
[17] H. Wagenblast, F. Fujita, and A. Damask, Acta Metall. **12**, 347 (1964).
[18] K. Tapasa, A. Barashev, D. Bacon, and Y. Osetsky, Acta Mater. **55**, 1 (2007).
[19] A. L. Nikolaev and T. E. Kurennykh, J. Nucl. Mater. **414**, 374 (2011).
[20] A. F. Bialon, T. Hammerschmidt, and R. Drautz, Phys. Rev. B **87**, 104109 (2013).
[21] P. Liu, W. Xing, X. Cheng, D. Li, Y. Li, and X.-Q. Chen, Phys. Rev. B **90**, 024103 (2014).
[22] S. Shang, H. Fang, J. Wang, C. Guo, Y. Wang, P. Jablonski, Y. Du, and Z. Liu, Corrosion Sci. **83**, 94 (2014).
[23] C.-C. Fu, J. Dalla Torre, F. Willaime, J. Bocquet, and A. Barbu, Nature Mater. **4**, 68 (2005).
[24] T. Jourdan, G. Bencteux, and G. Adjanor, J. Nucl. Mater. **444**, 298 (2014).
[25] J. Soler, E. Artacho, J. Gale, A. Garcia, J. Junquera, P. Ordejon, and D. Sanchez-Portal, J. Phys.: Condens. Matter **14**, 2745 (2002).
[26] J. P. Perdew, K. Burke, and M. Ernzerhof, Phys. Rev. Lett. **77**, 3865 (1996).
[27] E. Hayward and C.-C. Fu, Phys. Rev. B **87**, 174103 (2013).
[28] M. Methfessel and A. T. Paxton, Phys. Rev. B **40**, 3616 (1989).
[29] H. Jonsson, G. Mills, and K. W. Jacobsen, in *Classical and Quantum Dynamics in Condensed Phase Simulations* (World Scientific, Singapore, 1998), Chap. 16, pp. 385–404.
[30] C.-C. Fu and F. Willaime, Phys. Rev. B **72**, 064117 (2005).
[31] A. Krasheninnikov, P. Lehtinen, A. Foster, and R. Nieminen, Chem. Phys. Lett. **418**, 132 (2006).
[32] E. Meslin, C. C. Fu, A. Barbu, F. Gao, and F. Willaime, Phys. Rev. B **75**, 094303 (2007).
[33] N. Juslin and K. Nordlund, J. Nucl. Mater. **382**, 143 (2008).
[34] F. Djurabekova, L. Malerba, R. Pasianot, P. Olsson, and K. Nordlund, Philos. Mag. **90**, 2585 (2010).
[35] E. Martinez, O. Senninger, C.-C. Fu, and F. Soisson, Phys. Rev. B **86**, 224109 (2012).
[36] F. Nichols, J. Nucl. Mater. **75**, 32 (1978).
[37] K. Russell, Acta Metall. **19**, 753 (1971).
[38] Y. Jiang, J. R. Smith, and G. R. Odette, Phys. Rev. B **79**, 064103 (2009).
[39] D. E. Jiang and E. A. Carter, Phys. Rev. B **67**, 214103 (2003).
[40] G. Williamson and R. Smallman, Acta Crystallogr. **6**, 361 (1953).
[41] The phonons were calculated by the finite difference method implemented in SIESTA in the quasiharmonic approximation. We calculate the force constant matrix, or Hessian, by displacing each atom in the system by 0.04 Bohr in six directions. The convergence criteria for the force is 0.0015 eV/Å and for the stresses is 2.5 kbar.
[42] C. Domain and C. S. Becquart, Phys. Rev. B **65**, 024103 (2001).

[43] C. Becquart and C. Domain, Curr. Opin. Solid State Mater. Sci. **16**, 115 (2012).

[44] M. Nastar, Philos. Mag. **85**, 3767 (2005).

[45] T. Garnier, M. Nastar, P. Bellon, and D. R. Trinkle, Phys. Rev. B **88**, 134201 (2013).

[46] L. Messina, M. Nastar, T. Garnier, C. Domain, and P. Olsson, Phys. Rev. B **90**, 104203 (2014).

[47] G. Kresse and J. Hafner, Phys. Rev. B **47**, 558 (1993).

[48] G. Kresse and J. Hafner, Phys. Rev. B **49**, 14251 (1994).

[49] G. Kresse and J. Hafner, J. Phys.: Condens. Matter **6**, 8245 (1994).

[50] E. A. Brandes, *Smithells Metals Reference Book* (Butterworths, United Kingdom, 1983).

[51] J. da Silva and R. B. McLellan, Mater. Sci. Eng. **26**, 83 (1976).

[52] Landolt and Bornstein, *Diffusion in Solid Metals and Alloys*, edited by H. Mehrer (Springer-Verlag, Berlin, 1990).